# A versatile approach to the fabrication of $TiO_2$ nanostructures with reverse morphology and mesoporous Ag/$TiO_2$ thin films *via* cooperative PS-*b*-PEO self-assembly and a sol-gel process†

**Min-Ah Cha,[a] Changhak Shin,[b] Dinakaran Kannaiyan,[a] Yoon Hee Jang,[a] Saji Thomas Kochuveedu,[a] Du Yeol Ryu[b] and Dong Ha Kim*[a]**

***Received 20th April 2009, Accepted 29th July 2009***
***First published as an Advance Article on the web 25th August 2009***
**DOI: 10.1039/b907922j**



Hybrid titanium dioxide ($TiO_2$) nanostructures with engineered morphologies were produced by a simple synthetic approach based on cooperative sol-gel chemistry and self-assembly of amphiphilic poly(styrene-*block*-ethylene oxide) (PS-*b*-PEO) block copolymer (BCP) *via* spin-coating common solutions of BCP and inorganic precursors. $TiO_2$ nanostructures with two extreme reverse morphologies, *i.e.*, $TiO_2$ dot-in-PS matrix and PS dot-in-$TiO_2$ matrix, were obtained by increasing the volumetric ratio of the $TiO_2$ sol-gel precursor from 10 to 50 vol%. Incorporation of silver nitrate into the $TiO_2$ matrix afforded a hybrid Ag/$TiO_2$ thin film with hexagonally packed arrays of PS nanodots. Upon removal of the PS-*b*-PEO template from the initial hybrid films by UV treatment, inorganic nanostructures having the same lateral morphologies as the initial films were derived. Among the structures investigated, the Ag/$TiO_2$ mesoporous film exhibited the best photocatalytic performance. The surface/internal morphology and the mechanism of structural evolution were investigated by atomic force microscopy (AFM), transmission electron microscopy (TEM), and grazing-incidence small-angle X-ray scattering (GISAXS).

## Introduction

Recently, titanium dioxide ($TiO_2$) has been recognized as one of the most effective metal oxide materials due to its high photocatalytic efficiency, photochemical stability, non-toxic nature, and low cost. With these advantages, $TiO_2$ nanomaterials have been widely used in practical applications such as photocatalysis, chemical sensors, and solar cells.[1–5] In the numerous attempts made to enhance the performance of these nanomaterials, attention has focused on controlling and optimizing the composition, size and shape. Appropriate control of these properties, especially for the morphology and composition, has become a critical issue in this performance enhancement. Nanostructured $TiO_2$ materials with different shapes, including nanoparticles (NPs), nanotubes, nanowires, nanorods and thin films, have been synthesized by various specially tailored strategies, including hydrothermal synthesis, metal–organic chemical vapor deposition, and sol-gel template methods.[6–9]

The synthesis of nanomaterials through self-assembly (SA) involves the spontaneous and reversible organization of small building blocks for preparing a larger structure.[10] A block copolymer (BCP), composed of two different polymers covalently connected at one end, is a representative example of SA systems.[11–13] It provides a unique, versatile platform on which numerous types of hybrid organic–inorganic nanostructures can be derived. Among these, sol-gel chemistry using BCP self-assembly as a structure-directing agent is a well established strategy for the design of various hybrid nanostructures.[14–17] Using this method, Kim *et al.* recently reported that well-defined, periodic BCP/titania nanostructures could be prepared by one-step spin-coating of a common solution consisting of poly-styrene-*block*-poly(ethylene oxide) (PS-*b*-PEO) and $TiO_2$ sol-gel precursor. Hexagonally ordered arrays of titania nanodots with controlled size and spacing were acquired after removing the organic template from the initial hybrid. Morphological evolution, crystallinity, and photoluminescence were investigated for the titania nanodot arrays thus prepared.[18–21] In a similar vein, other researchers have reported on the fabrication of mesoporous $TiO_2$ film[22] and on its integration into a photovoltaic cell[23] based on the combination of BCP SA and sol-gel chemistry.

However, in our previous studies we did not discuss the hybrid film morphology with the relative amount of $TiO_2$ sol-gel precursor to BCP solution higher than 40 vol%.[18–21] In this paper, we show that morphological inversion occurs at a higher relative amount of $TiO_2$ sol-gel precursor. By comparison, a photolithographic approach to the fabrication of positive and negative $TiO_2$ micropatterns has been reported recently.[24] We also demonstrate that stable, mixed nanodot/nanowire morphologies are obtained at intermediate $TiO_2$ sol-gel precursor amounts. Finally, we expand this methodology to fabricate a mesoporous Ag/$TiO_2$ film with improved photocatalytic properties and discuss the mechanism of its enhancement. This series of hybrid

[a]*Department of Chemistry and Nano Science, Ewha Womans University, 11-1 Daehyun-dong, Seodaemun-gu, Seoul, 120-750, Korea. E-mail: dhkim@ewha.ac.kr; Fax: +82-2-3277-3419; Tel: +82-2-3277-4517*
[b]*Department of Chemical and Biomolecular Engineering, Yonsei University, 262 Seongsanno, Seodaemun-gu, Seoul, 120-749, Korea. E-mail: dyryu@yonsei.ac.kr; Fax: +82-2-312-6401; Tel: +82-2-2123-5756*
† Electronic supplementary information (ESI) available: AFM images. See DOI: 10.1039/b907922j

nanostructures was investigated by microscopic studies, grazing-incidence small-angle X-ray scattering (GISAXS), and photocatalytic properties.

## Experimental section

### Chemicals and materials

PS-*b*-PEO (6500–20 000 g/mol, PDI = 1.06) was purchased from Polymer Source Inc. (Dorval, Canada) and used as provided. 1,4-Dioxane, concentrated hydrochloric acid (HCl, 37%), and isopropyl alcohol were purchased from Daejung Chemicals & Metals Co., Ltd. and used without further purification. Titanium tetraisopropoxide (TTIP) and silver nitrate ($AgNO_3$) were purchased from Sigma Aldrich Inc.

### Preparation of $TiO_2$ and Ag/$TiO_2$ thin films

As the matrix polymer, an amphiphilic, asymmetric PS-*b*-PEO diblock copolymer was dissolved in 1,4-dioxane at 1 wt% concentration at room temperature under stirring. $TiO_2$ sol-gel precursor composed of 0.25 g concentrated HCl, 5 ml isopropyl alcohol, and 0.71 g TTIP was stirred for more than 1 h at room temperature. The hydrophilic titania sol-gel precursor selectively infiltrates into hydrophilic PEO domains and forms titania nanostructures by gelation. By varying the volumetric ratio of the sol-gel precursor to polymer solution from 10 to 50 vol%, diverse surface morphologies such as nanodots, nanowires, and mesoporous structures were induced. In order to prepare hybrid Ag/$TiO_2$ film, a 1 wt% solution of $AgNO_3$ in isopropyl alcohol was added into a PS-*b*-PEO solution containing 50 vol% $TiO_2$ sol-gel precursor. The final common solution was stirred for more than 12 h and spin-coated onto Si wafers at 2500 rpm for 60 s on a Spin-1200D (Midas System Inc.) spin-coater.

### Grazing incidence small-angle X-ray scattering (GISAXS)

GISAXS measurements were conducted at the synchrotron facility (4C2 beam-lines) of the Pohang Accelerator Laboratory, Korea. The operating conditions were set to a wavelength of 1.38 Å and a sample-to-detector distance of 2.3 m. The incident angles were set at 0.18 and 0.14° to probe the internal structures and the surface of the entire film by enabling the X-rays to pass through the thin film above the critical angle ($\alpha_c$) of the film samples. 2D GISAXS patterns were recorded using a CCD detector (Princeton Instruments) positioned at the end of a vacuum guide tube with an exposure time of 10–60 s.

### Photocatalytic activities

A methylene blue (MB) solution was prepared by dissolving 5 ppm of MB powder in distilled water. A fixed amount of this solution was poured into each quartz cuvette. Si wafers coated with $TiO_2$ nanostructures were placed at the bottom of the cuvettes filled with MB solution. Each cuvette containing $TiO_2$ nanocatalysts was exposed to UV light of wavelength 254 nm for 120 min. The absorbance of the MB solution irradiated by UV light was measured every 30 min by UV-vis spectrometry. An MB solution containing blank Si wafer was used as a control.

### Instruments and measurements

The surface morphologies of the nanostructured thin films on Si wafers were analyzed with an atomic force microscope (AFM) in tapping mode (Digital Instruments Dimension 3100 scanning force microscope). High-resolution transmission electron microscopy (HRTEM) and energy-dispersive X-ray spectroscopy (EDX) measurements were carried out on a JEOL JSM2100-F at 100 kV. Samples for HRTEM were prepared by the following procedure. A thin carbon layer was coated onto the surface of the hybrid films on Si wafers. Then a poly(vinyl alcohol) layer was deposited onto the carbon layer. Subsequently the multilayer sample was detached from the Si wafers and floated on a water surface with the hybrid film side on the top. Finally, the films were picked up using TEM grids. To remove the polymer matrix from the hybrid thin film, the spin-coated samples were irradiated by UV light of wavelength 254 nm with a dose of 25 J $cm^{-2}$ (XX-15S; UVP, Inc.) at room temperature for 5 h.

## Results and discussion

Scheme 1 shows the overall fabrication process for the titania nanostructures templated by PS-*b*-PEO/$TiO_2$ sol-gel precursor. A 1,4-dioxane solution of PS-*b*-PEO was mixed with the desired amount of sol-gel precursor solution to induce nanodot (10 vol%), mixed (20 vol%), and inverse nanodot (50 vol%) patterns. The yellow and blue regions represent the PS and PEO-$TiO_2$ domains, respectively. With 20 vol% $TiO_2$ sol-gel precursor, the surface morphology showed irregular morphology. With 10 and 50 vol% $TiO_2$, the as-cast samples appeared quite similar, with both showing hexagonally packed nanodot arrays. In between these two, the structural conversion from $TiO_2$ nanodot to PS nanodot occurred with increasing relative volume ratio of one block to another. The initial hybrid films were then exposed to UV light to obtain $TiO_2$ nanostructures without organic components. As shown at the bottom in Scheme 1, a series of $TiO_2$ nanostructures with engineered morphologies, *i.e.*, nanodot, mixed nanodot/nanowire and mesoporous $TiO_2$, were obtained. By introducing $AgNO_3$ to the PS-*b*-PEO/$TiO_2$ nanostructure with a fixed amount of sol-gel precursor at 40 vol%, a hybrid Ag/$TiO_2$ mesoporous thin film was also obtained. The surface morphology of the $AgNO_3$-containing structure was similar to the one without $AgNO_3$. The surface of the films was examined by microscopy and EDX spectroscopy. The photocatalytic property was compared for the Ag-containing and pure $TiO_2$ nanostructures.

A series of height-contrast AFM images of PS-*b*-PEO films with $TiO_2$ sol-gel content ranging from 0–50 vol% are shown in Fig. 1. A comparison of the four morphologies revealed the strong dependence of the nanostructure formation on the relative amount of sol-gel precursor in the common solution. The surface of the pristine PS-*b*-PEO film exhibited a mixed morphology of nanodots and nanowires, as shown in Fig. 1A. The morphology of the film with 10 vol% precursor in Fig. 1B shows typical hexagonal arrays of $TiO_2$ nanodots protruded from the surface of the BCP matrix. This result is consistent with that in our previous study.[17] Further increasing the precursor to an intermediate level (20 vol%) restored the surface texture to a mixed morphology consisting of nanodots and short nanowires

 

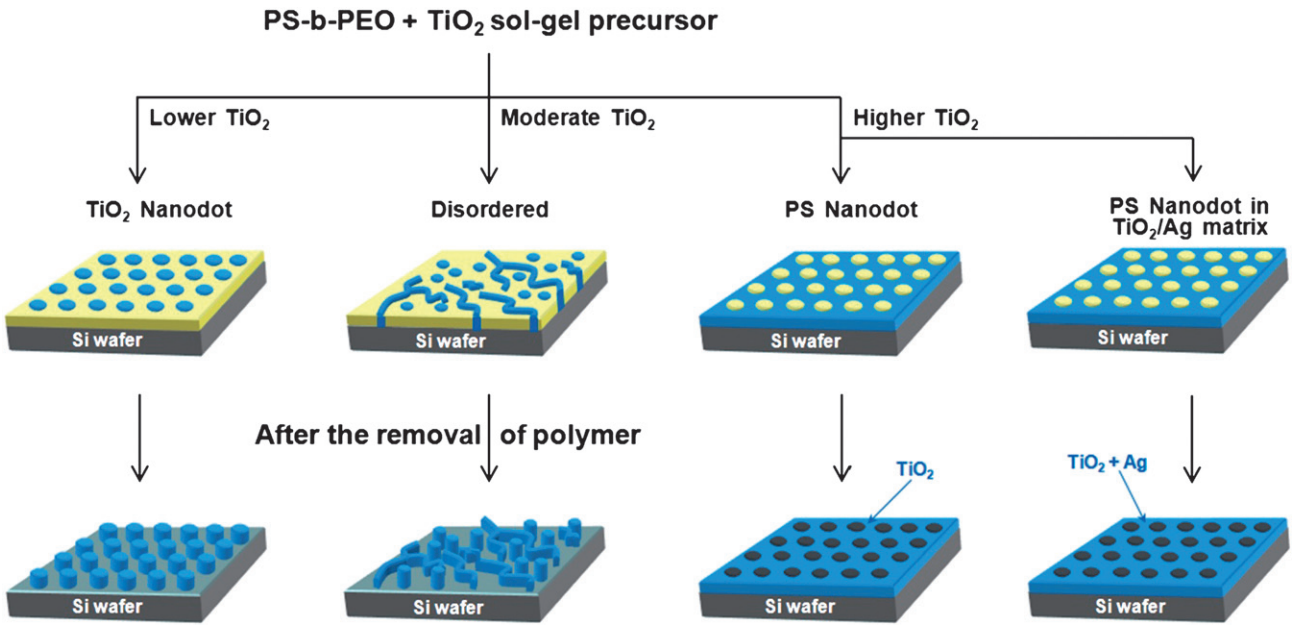


**Scheme 1** Schematic diagram of the fabrication process used to generate $TiO_2$ nanodot, mixed $TiO_2$ nanodot/wire and mesoporous $TiO_2$ film templated by PS-*b*-PEO/sol-gel films. A 1,4-dioxane solution of PS-*b*-PEO was mixed with the desired amount of the sol-gel precursor solution. 1 wt% of $AgNO_3$ solution in isopropanol was added to the solution of mesoporous $TiO_2$ film in order to prepare hybrid mesoporous $Ag/TiO_2$ film.

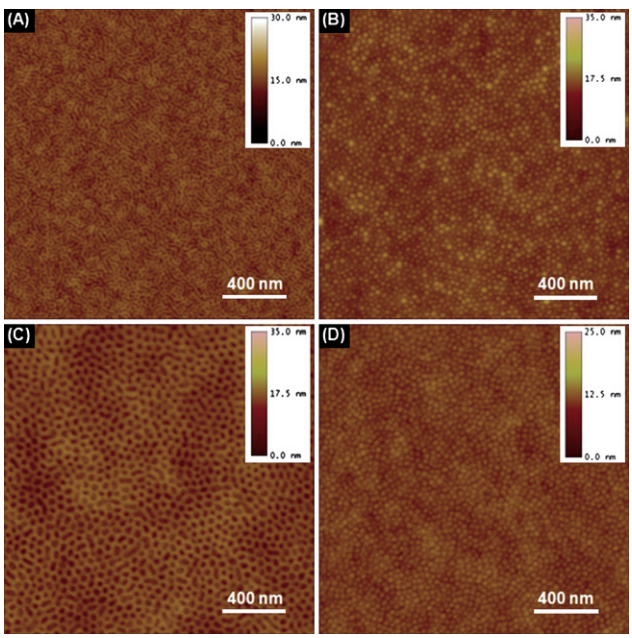


**Fig. 1** Height-contrast AFM images of nanoscopic entities of $TiO_2$ in PS-*b*-PEO thin films with different relative amounts of $TiO_2$ sol-gel precursor: (a) 0 vol%, (b) 10 vol%, (c) 20 vol% and (d) 50 vol%.

(Fig. 1C), implying that the film underwent a transient state. The hybrid film with a greater amount of precursor (50 vol%) displayed well-defined nanodot morphology again, while the height contrast was completely reversed due to the real phase inversion. The driving force to the more directed morphology with increasing precursor content, in comparison to the random nanodomain orientations of the pristine PS-*b*-PEO film, was attributed to the increased repulsion between PS and the precursor-containing PEO phases. This suggested that a systematic morphological transformation occurred with increasing precursor amount, although the series of films with different precursor amounts were seemingly similar each other (between A and C; between B and D). We further discuss their internal structures below, along with the GISAXS studies.

Fig. 2A–D shows the corresponding series of phase-contrast AFM images of thin films with different sol-gel precursor

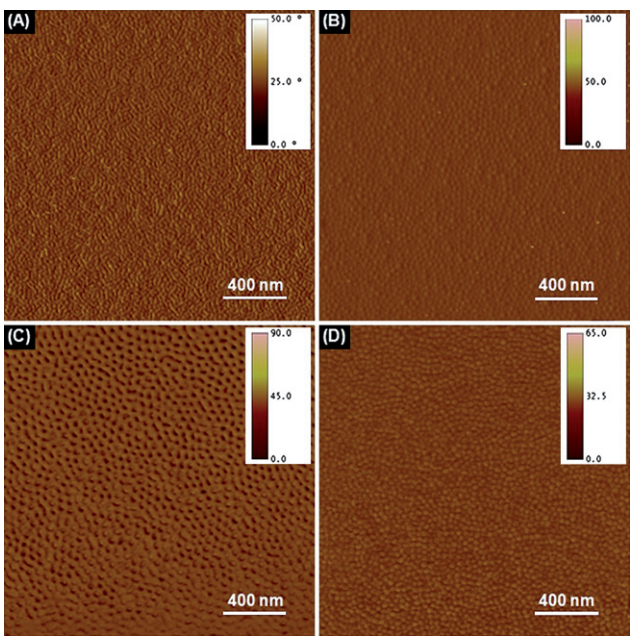


**Fig. 2** Phase-contrast AFM images of nanoscopic entities of $TiO_2$ in PS-*b*-PEO thin films with different relative amounts of $TiO_2$ sol-gel precursor: (a) 0 vol%, (b) 10 vol%, (c) 20 vol% and (d) 50 vol%.

amounts. The brighter part represents domains with larger modulus in the phase-contrast image. All phase images had similar morphologies to the corresponding height images shown in Fig. 1. The nanodot arrays in Fig. 2B and 2D have almost the same size and periodicity. This raises a question as to the composition of the matrix and of the circular domain of the films in Fig. 2D, considering that it contains 50 vol% $TiO_2$ sol-gel precursor solution. In order to clarify this issue, the polymer matrix was eliminated by exposing the films to UV and the resulting pure $TiO_2$ nanostructures were examined by AFM, as shown in Fig. 3.

In Fig. 3A, arrays of $TiO_2$ dots are observed with a clear boundary compared with its parent morphology (Fig. 1B) after the elimination of the polymer matrix. The hybrid film with 20 vol% precursor (Fig. 1C) produced distinct $TiO_2$ nanopatterns mainly composed of nanodots and locally existing nanowires. A dramatic inversion of the morphology occurred for the film with a higher precursor amount. As shown in Fig. 3C, quasi-hexagonal arrays of nanoscale pits in continuous $TiO_2$ film were observed at the initial positions of the minor PS domains in Fig. 1D, indicating that the PEO domains constituted the major component due to the significant swelling induced by the incorporation of the $TiO_2$ precursors. The arrays of indentations can be observed in the magnified image of a local area in Fig. 3C, along with a sectional profile (Fig. 3D).

The AFM results provide local information obtained from a relatively small, micrometer scale, area of the surface. GISAXS techniques were employed to complement the microscopic studies and perform more in-depth analysis on the structural evolution of the films over a large area of the films in both lateral and thickness directions. 2D GISAXS patterns for PS-*b*-PEO and hybrid PS-*b*-PEO/$TiO_2$ films on the Si substrate are shown in Fig. 4. In the scattering geometry used, $q_y$ is the scattering vector normal to the plane of incidence (parallel to the film surface), where the d-spacing is related to $q_y$ by $d = 2\pi/q_y^{max}$. $q_z$ is the scattering vector normal to the sample surface, defined as $q_z = (4\pi/\lambda)\sin 2\theta$, where $\lambda$ is the wavelength of the X-rays and $2\theta$ is the scattering angle. The GISAXS pattern for the pristine PS-*b*-PEO film in Fig. 4A shows a lower intensity of the in-plane scattering peaks at $q_y = 0.219$ nm$^{-1}$ along constant $q_z = 0.288$ nm$^{-1}$ due to the low electron-density contrast between the PS and PEO blocks. The Bragg rod pattern at $q_y = 0.219$ nm$^{-1}$ indicates PEO microdomains oriented normal to the film surface with a *d*-spacing of 28.6 nm, representing the average periodicity of mixed nanodot/nanowire patterns. This result led us to conclude that most of the PEO domains span the entire thickness of the film with a perpendicular orientation, although nanowire PEO domains are found locally. For the hybrid PS-*b*-PEO/$TiO_2$ film with 10 vol% $TiO_2$, the in-plane

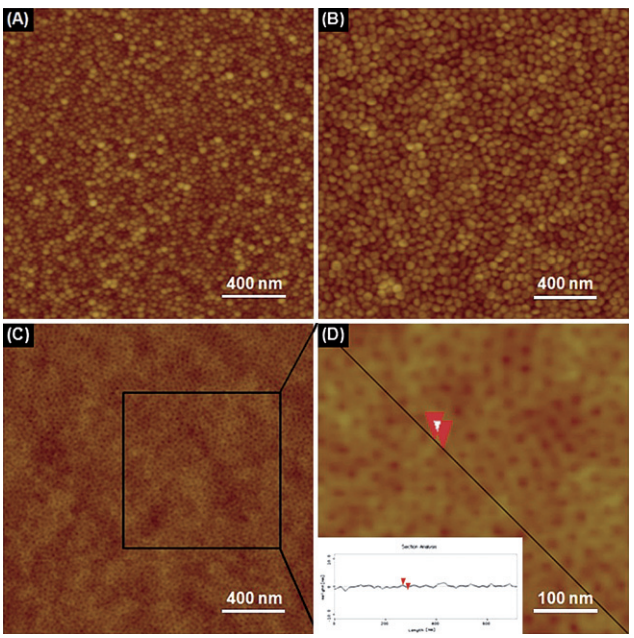


**Fig. 3** Height-contrast AFM images of pure $TiO_2$ nanostructures obtained from the parent hybrid films with different amounts of $TiO_2$ sol-gel precursor after UV exposure: (a) 10 vol%, (b) 20 vol% and (c) 50 vol%. (d) A magnified image of a selected region in (c) along with a sectional line profile (inset).

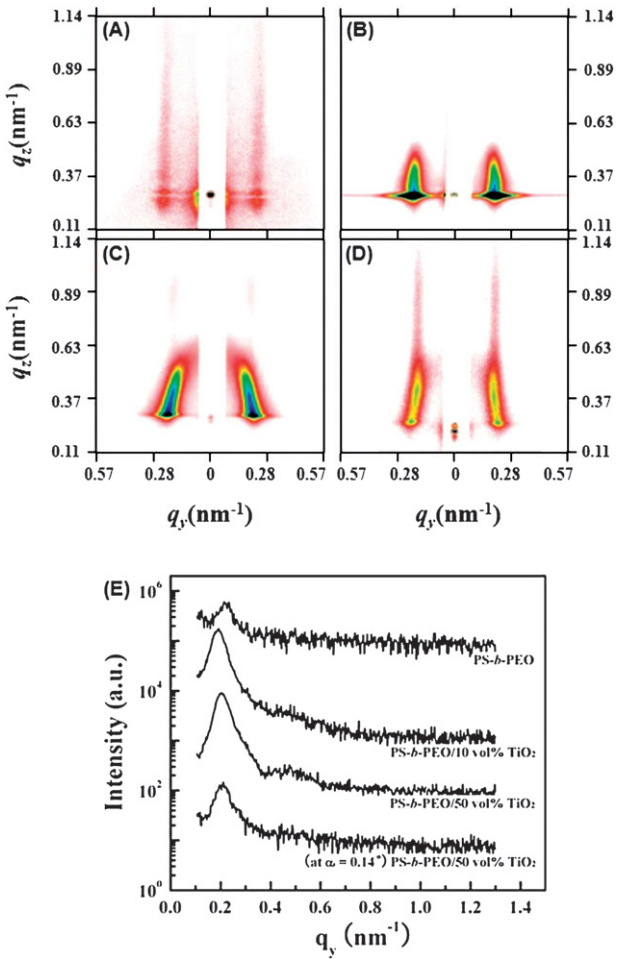


**Fig. 4** 2D-GISAXS patterns at incident angles of 0.18° (a, b, and c) and 0.14° (d) for PS-*b*-PEO (a) and hybrid PS-*b*-PEO/$TiO_2$ films with 10 vol% of $TiO_2$ (b) and 50 vol% of $TiO_2$ (c and d) on the Si substrate. The incident angles were set at 0.18° and 0.14° to probe the internal structures and the surface of the entire film. Intensity profiles (e) are scanned at constant $q_z = 0.288$ nm$^{-1}$ (at $q_z = 0.222$ nm$^{-1}$ for the pattern (d) due to the different incident angle of 0.14°) from GISAXS patterns as a function of $q_y$.

 

scattering peaks at $q_y = 0.190$ nm$^{-1}$ were significantly intensified due to the increased electron-density contrast, having the same orientation as the cylindrical microdomain. Detailed line scans from the GISAXS patterns, scanned along the $q_y$-direction at constant $q_z = 0.288$ nm$^{-1}$, are shown in Fig. 4E, which reflect the structural changes from the PS-*b*-PEO film. The addition of 10 vol% $TiO_2$ increased the *d*-spacing of the microdomain from 28.6 nm to 33.1 nm, as evidenced by the peak shift from $q_y = 0.219$ nm$^{-1}$ to 0.190 nm$^{-1}$ ($d = 2\pi/q_y^{max}$). This phenomenon was attributed to the preferential segregation of $TiO_2$ to the cylindrical PEO microdomains through the coordinative interaction. Further increasing the amount of $TiO_2$ up to 50 vol%, as shown in Fig. 4(C and E), enhanced the scattering peaks at $q_y = 0.205$ nm$^{-1}$ corresponding to a *d*-spacing of 30.6 nm, although the slightly bent scattering patterns to a lower *q* value indicated that most of the cylindrical microdomains were oriented normal to the film surface. Here, in the hybrid PS-*b*-PEO/$TiO_2$ with 50 vol% $TiO_2$, a phase inversion occurred with the addition of a relatively large amount of $TiO_2$ due to the increased volume fraction of PEO-$TiO_2$ (refer to the AFM images in Fig. 1D and 2D). Accordingly, the GISAXS patterns for hybrid PS-*b*-PEO/$TiO_2$ with 50 vol% $TiO_2$ revealed that the PS microdomains were still oriented normal to the film surface, where $TiO_2$ is randomly dispersed in the PEO matrix of the entire film. In addition to the internal structures of the entire film, the GISAXS pattern at an incident angle of 0.14° in Fig. 4D confirmed the consistent morphologies between the surface and the internal structures.

In the hybridization of PS-*b*-PEO with $TiO_2$ precursor, the morphologies with a relatively low amount of $TiO_2$ precursor could not be obtained reproducibly when a series of samples were prepared at different times. This suggested that the hydrophilic PEO block was highly susceptible to the surrounding environment, in particular the relative humidity, at the immediate point of film preparation. On the other hand, the hybrid thin films containing more than 40 vol% $TiO_2$ precursor always showed the same, well-defined morphologies in a reproducible manner, implying that the labile PEO domains were stabilized by the inorganic precursors (see supporting information Figs. S1–S3†).

In order to demonstrate the versatility of this hybridization methodology, we extended the protocol for the synthesis of mesoporous $TiO_2$ films (Fig. 3C) to generate composite Ag/$TiO_2$ mesoporous film. To this end, silver nitrate ($AgNO_3$), a precursor of Ag, was additionally mixed with the PS-*b*-PEO/sol-gel precursor solution. Fig. 5A shows the AFM height-contrast image of the ternary hybrid film with an overall organization similar to that of the film in Fig. 1D, *i.e.*, arrays of PS nanodots in an inorganic matrix. UV treatment of the initial film simultaneously reduced $AgNO_3$ to metallic Ag and formed mesoporous Ag/$TiO_2$ film, as shown in Fig. 5B. In order to investigate the presence and spatial location of the Ag NPs, we performed TEM and EDX. Ag NPs were sporadically dispersed in the $TiO_2$ matrix film (Fig. 5C) and the EDX result confirmed the presence of Ag and Ti elements (Fig. 5D).

Finally, we evaluated the performance of three different types of $TiO_2$ nanostructure in terms of photocatalysis. Photocatalytic activities were examined by degradation of MB solution. The characteristic absorption of MB in the UV-visible spectrum was monitored to determine the effect of the $TiO_2$ nanocatalysts on

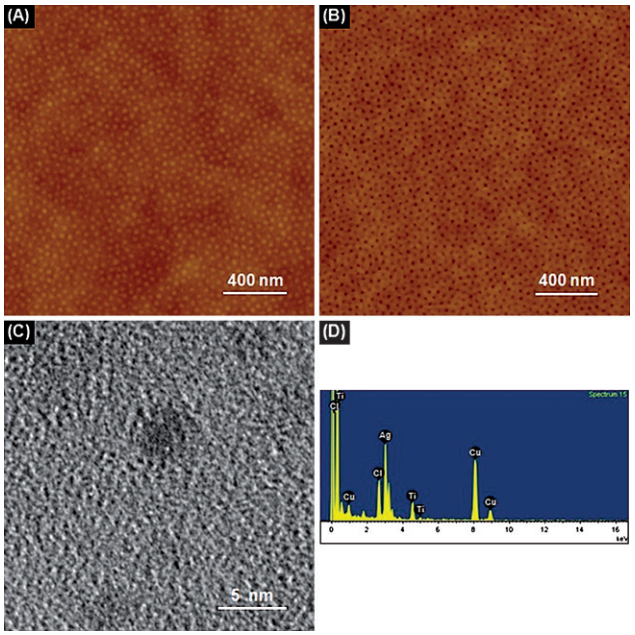


**Fig. 5** Height-contrast AFM images of a PS-*b*-PEO film containing 50 vol% $TiO_2$ sol-gel precursor and $AgNO_3$ (molar ratio, Ag/EO = 0.5): (a) initial hybrid film, (b) hybrid mesoporous Ag/$TiO_2$ nanostructure after UV treatment, (c) TEM image of (a), and (d) EDX analysis.

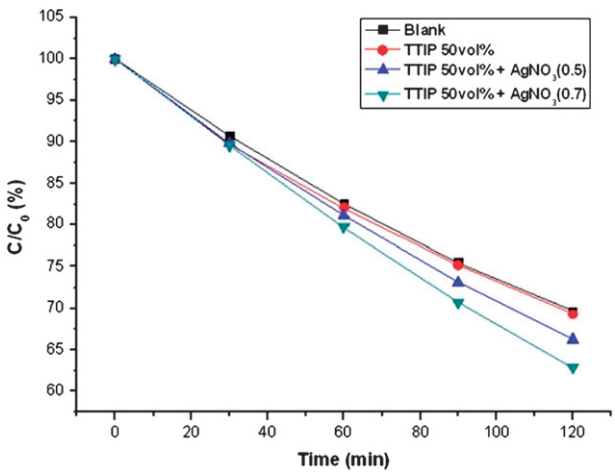


**Fig. 6** Photocatalytic activities of hybrid nanostructures in terms of the degradation of methylene blue (MB) as a function of reaction time. The samples used were mesoporous $TiO_2$ film (●), and two mesoporous $TiO_2$ films with a $AgNO_3$ molar ratio of 0.5 (Ag/EO = 0.5) (▲) and 0.7 (Ag/EO = 0.7) (▼).

the MB concentration. Hybrid mesoporous Ag/$TiO_2$ films with two different amounts of Ag NPs were compared with pure mesoporous $TiO_2$ film. The overall rate of MB degradation in the pure mesoporous $TiO_2$ film was almost the same as that of the control sample, whereas the mesoporous $TiO_2$ films containing Ag NPs showed enhanced efficiency. In such a hybrid metal/$TiO_2$ system, more than one mechanism may be involved in the enhancement of photocatalytic activity. The dye degradation results from the self-degradation of the oxidized dye molecules following the charge transfer from the excited dye to the $TiO_2$

catalyst induced by UV light irradiation.[25,26] In addition to this primary effect, the modification of the semiconductor by dispersed Ag NPs in the mesoporous $TiO_2$ film provides a more effective pathway for light-induced dye degradation reactions due to the increased number of active sites generated with the assistance of holes and electrons at the interface between $TiO_2$ and metal NPs.[26–30] On the surface of the hybrid Ag–$TiO_2$ catalyst, recombination of electron–hole pairs is inhibited by the migration of photo-induced electrons from the $TiO_2$ surface to the Ag metal. The film with more Ag moieties, *i.e.*, containing a lower concentration of holes for recombination, facilitated the degradation more efficiently than the film with less Ag, as shown in Fig. 6. Importantly, the degree of enhancement of the photocatalytic activity upon hybridization with Ag remained marginal. This was ascribed to the limited amount and surface area of the hybrid system in a monolayer film. We expect that the integration of this type of hybrid into 3-D geometry will enhance the activity.

## Conclusions

In this study, we synthesized three different configurations of $TiO_2$ nanostructures, *i.e.*, arrays of $TiO_2$ nanodots, mesoporous $TiO_2$ and Ag/$TiO_2$ thin films, *via* the cooperative self-assembly of PS-*b*-PEO and a sol-gel process. With increasing content of $TiO_2$ sol-gel precursor relative to PS-*b*-PEO, morphological inversion was induced from the inorganic nanodot arrays in the PS matrix to PS nanodot arrays in the inorganic matrix due to the significant increase in the relative volume of PEO-$TiO_2$ domains in the entire system. Subsequent elimination of the polymer template generated pure $TiO_2$ nanodot arrays and mesoporous $TiO_2$ thin films. Hybrid Ag/$TiO_2$ mesoporous films were also obtained by incorporating a second inorganic precursor into the hydrophilic PEO domains. The structural evolution of the hybrid nanostructures and the internal structures of the resulting nanostructures were monitored by AFM, TEM and GISAXS studies, and the observations were complementary. As for the function of the inorganic nanostructures, the photocatalytic activity of the mesoporous $TiO_2$ thin film was evaluated to be better than that of the $TiO_2$ nanodot arrays, and was markedly increased upon the incorporation of Ag NPs into the mesoporous $TiO_2$ matrix. This rational design of hybrid metal/$TiO_2$ nanostructures based on BCP templating in conjunction with sol-gel chemistry may establish a generalized fabrication protocol for a wide spectrum of inorganic hybrid mesoporous materials.

## Acknowledgements

This work was supported by grants from the Korea Science and Engineering Foundation (KOSEF) funded by the Korea government (MEST) (No. R11-2005-008-00000-0 and R01-2008-000-11712-0). DYR acknowledges the support of the APCPI ERC program (R11-2007-050-01004) funded by the Ministry of Education, Science & Technology (MEST), Korea.

## References

1 D. T. On, *Langmuir*, 1999, **15**, 8561.
2 Q. Dai, Z. Zhang, N. He, P. Li and C. Yuan, *Mater. Sci. Eng., C*, 1999, **8–9**, 417.
3 Y. Wang, X. Tang, L. Yin, W. Huang, Y. R. Hacohen and A. Gedanken, *Adv. Mater.*, 2000, **12**, 1183.
4 H. S. Zhou and I. Honma, *Mater. Res. Soc. Symp. Proc.*, 1999, **516**, 209.
5 V. F. Stone, Jr. and R. J. Davis, *Chem. Mater.*, 1998, **10**, 1468.
6 Y. Kotani, T. Matoda, A. Matsuda, T. Kogure, M. Tatsumisago and T. Minami, *J. Mater. Chem.*, 2001, **11**, 2045.
7 P. D. Cozzoli, A. Kornowski and H. Weller, *J. Am. Chem. Soc.*, 2003, **125**, 14539.
8 P. D. Yang, D. Y. Zhao, D. I. Margolese, B. F. Chmelka and G. D. Stucky, *Nature*, 1998, **396**, 152.
9 Y. F. Lu, R. Ganguli, C. A. Drewien, M. T. Anderson, C. J. Brinker, W. L. Gong, Y. X. Guo, H. Soyez, B. Dunn, M. H. Huang and J. I. Zink, *Nature*, 1997, **389**, 364.
10 M. Boncheva and G. M. Whitesides, *MRS Bull.*, 2005, **30**, 736.
11 F. S. Bates and G. H. Fredrickson, *Annu. Rev. Phys. Chem.*, 1990, **41**, 525.
12 M. J. Fasolka and A. M. Mayes, *Annu. Rev. Phys. Chem.*, 2001, **31**, 323.
13 I. W. Hamley, *The Physics of Block Copolymers*, Oxford University Press, Oxford, 1998.
14 M. Templin, A. Franck, A. D. Chesne, H. Leist, Y. Zhang, R. Ulrich, V. Schaedler and U. Wiesner, *Science*, 1997, **278**, 1795.
15 C. Sanchez, C. Boissiere, D. Grosso, C. Laberty and L. Nicole, *Chem. Mater.*, 2008, **20**, 682.
16 D. Zhao, J. Feng, Q. Huo, N. Melosh, G. H. Fredrickson, B. F. Chmelka and G. D. Stucky, *Science*, 1998, **279**, 548.
17 K. Yu, A. J. Hurd, A. Eisenberg and C. J. Brinker, *Langmuir*, 2001, **17**, 7961.
18 D. H. Kim, Z. Sun, T. P. Russell, W. Knoll and J. S. Gutmann, *Adv. Funct. Mater.*, 2005, **15**, 1160.
19 Z. Sun, D. H. Kim, M. Wolkenhauer, G. G. Bumbu, W. Knoll and J. S. Gutmann, *ChemPhysChem*, 2006, **7**, 370.
20 J. Peng, W. Knoll, C. Park and D. H. Kim, *Chem. Mater.*, 2008, **20**, 1200.
21 X. Lie, J. Peng, J.-H. Kang, J.-H. Choy, M. Steinhart, W. Knoll and D. H. Kim, *Soft Matter*, 2008, **4**, 515.
22 J. Perlich, M. Memesa, A. Diethert, E. Metwalli, W. Wang, S. V. Roth, A. Timmann, J. S. Gutmann and P. Muller-Buschbaum, *ChemPhysChem*, 2009, **10**, 799.
23 B. Ma, J. Ma and G. K. L. Goh, *J. Mater. Sci.*, 2008, **43**, 4297.
24 P. Yang, M. Yang, S. Zou, J. Xie and W. Yang, *J. Am. Chem. Soc.*, 2007, **129**, 1541.
25 J. Peng, X. Li, D. H. Kim and W. Knoll, *Macromol. Rapid Commun.*, 2007, **28**, 2055.
26 S. Anandan, P. S. Kumar, N. Pugazhenthiran, J. Madhavan and P. Maruthamuthu, *Sol. Energy Mater. Sol. Cells*, 2008, **92**, 929.
27 Y. Zheng, L. Zheng, Y. Zhan, X. Lin, Q. Zheng and K. Wei, *Inorg. Chem.*, 2007, **46**, 6980.
28 P. K. Sudeep, K. Takechi and P. V. Kamat, *J. Phys. Chem. C*, 2007, **111**, 488.
29 T. Hirakawa and P. V. Kamat, *J. Am. Chem. Soc.*, 2005, **127**, 3928.
30 J. Ryu and W. Choi, *Environ. Sci. Technol.*, 2004, **38**, 2928.

 